CELL BIOLOGY

P2X4 and P2X7 are essential players in basal T cell activity and Ca^{2+} signaling milliseconds after T cell activation

Valerie J. Brock[1], Insa M. A. Wolf[1], Marco Er-Lukowiak[2], Niels Lory[3], Tobias Stähler[3], Lena-Marie Woelk[4], Hans-Willi Mittrücker[3], Christa E. Müller[5], Friedrich Koch-Nolte[3], Björn Rissiek[2], René Werner[4], Andreas H. Guse[1], Björn-Philipp Diercks[1]*

Initial T cell activation is triggered by the formation of highly dynamic, spatiotemporally restricted Ca^{2+} microdomains. Purinergic signaling is known to be involved in Ca^{2+} influx in T cells at later stages compared to the initial microdomain formation. Using a high-resolution Ca^{2+} live-cell imaging system, we show that the two purinergic cation channels P2X4 and P2X7 not only are involved in the global Ca^{2+} signals but also promote initial Ca^{2+} microdomains tens of milliseconds after T cell stimulation. These Ca^{2+} microdomains were significantly decreased in T cells from *P2rx4*$^{-/-}$ and *P2rx7*$^{-/-}$ mice or by pharmacological inhibition or blocking. Furthermore, we show a pannexin-1–dependent activation of P2X4 in the absence of T cell receptor/CD3 stimulation. Subsequently, upon T cell receptor/CD3 stimulation, ATP release is increased and autocrine activation of both P2X4 and P2X7 then amplifies initial Ca^{2+} microdomains already in the first second of T cell activation.

INTRODUCTION

Efficient immune response requires precisely coordinated signaling pathways, both for cell-to-cell communication and for intracellular signal transduction. Important examples for these molecules involved in T cell activation are Ca^{2+} ions that act intracellularly or adenosine triphosphate (ATP) as a proinflammatory purinergic mediator (*1*, *2*). The signaling pathways of these molecules are prominent targets for therapeutics (*3*–*6*). As T cell activation and signaling provide many potential spots for medical intervention, uncovering interactions between different signaling molecules will improve therapeutical approaches. T cell receptor (TCR)/CD3 complex–stimulated initial Ca^{2+} microdomains in T cells are evoked by the production of nicotinic acid adenine dinucleotide phosphate (NAADP), the most potent Ca^{2+}-mobilizing second messenger (*7*), targeting ryanodine receptor type 1 (RYR1). Furthermore, RYR1 and ORAI1 channels, the latter activated by clusters of "stromal interacting molecule" (STIM) 1 and 2, closely collaborate in this process, likely in endoplasmic reticulum (ER)–plasma membrane (PM) junctions (*8*, *9*). These initial Ca^{2+} microdomains are described as short-lived, highly dynamic Ca^{2+} signals with amplitudes of approximately 200 to 400 nM in primary mouse T cells arising in tens of milliseconds to seconds after stimulation of the TCR/CD3 complex (*8*, *9*). Furthermore, preformed clusters of STIM1 and ORAI1 were found in T cells, resulting in lower and less frequent Ca^{2+} microdomains already without direct stimulation of the TCR/CD3 complex, suggesting a low-grade preactivation of these cells (*9*). Recently, a long sought-after NAADP binding protein named "hematological and neurological expressed 1-like protein" (HN1L)/"Jupiter microtubule associated homolog 2" (JPT2) was found (*10*, *11*). Knockout (KO) of HN1L/JPT2 significantly reduced the number of Ca^{2+} microdomains in primary T cells (*10*), similar to inhibition of NAADP by NAADP antagonist BZ194 treatment or KO of RYR1 (*8*, *9*). Targeting NAADP signaling in a rat model of experimental autoimmune encephalomyelitis by BZ194 resulted in decreased proinflammatory cytokines and attenuated clinical symptoms (*6*).

P2X channels are ligand-gated ion channels activated by ATP (*12*–*14*). The two purinergic channels P2X4 and P2X7 have been shown to play an essential role in T cell function (*15*) and to amplify global Ca^{2+} signaling during T cell activation (*16*–*18*). Targeting P2X7 in a mouse model of contact hypersensitivity, a P2X7-inhibiting nanobody, namely, 13A7-HLE, decreased local inflammation by reducing inflammatory cytokine levels (*19*).

It is known that purinergic signaling is connected to Ca^{2+} signaling: An increasing Ca^{2+} concentration via store-operated Ca^{2+} entry (SOCE) through ORAI1 during T cell activation promotes the production of ATP inside the mitochondria immediately after TCR stimulation (*18*). ATP is transported to the cytosol and is subsequently released via pannexin-1 (PANX1) hemichannels, where it activates P2X4 and P2X7 channels in an autocrine manner, resulting in an influx of Ca^{2+}. These Ca^{2+} signals were visualized several minutes after TCR stimulation (*16*–*18*). Impaired purinergic signaling caused by inhibition of the P2X4 channel in human and mouse T cells prevents T cell proliferation and migration (*20*), demonstrating the important physiological role of purinergic signaling on general T cell function.

In the present study, by using *P2rx4*$^{-/-}$ and *P2rx7*$^{-/-}$ T cells or inhibiting compounds or nanobodies, we show that P2X4 and P2X7 are already involved in the initial step of T cell activation, the generation of initial Ca^{2+} microdomains tens of milliseconds after TCR stimulation. By inhibition of PANX1 or degradation of extracellular ATP, we demonstrate that PANX1 delivers ATP for the extracellular activation of the two P2X channels in this initial step of T cell activation. Moreover, we show that low-grade preactivation of unstimulated T cells not only is dependent on the interaction of STIM1 and ORAI1 (*9*) but also relies on basal ATP release via PANX1 and

[1]The Ca^{2+} Signalling Group, Department of Biochemistry and Molecular Cell Biology, University Medical Center Hamburg-Eppendorf, 20246 Hamburg, Germany. [2]Department of Neurology, University Medical Centre Hamburg Eppendorf, 20246 Hamburg, Germany. [3]Department of Immunology, University Medical Centre Hamburg Eppendorf, 20246 Hamburg, Germany. [4]Department of Computational Neuroscience, University Medical Centre Hamburg Eppendorf, 20246 Hamburg, Germany. [5]Department of Pharmacy, University of Bonn, 53121 Bonn, Germany.
*Corresponding author. Email: b.diercks@uke.de

autocrine activation of P2X4. Thus, our data indicate that purinergic signaling not only amplifies global Ca^{2+} events during T cell activation but also plays an essential role in fine-tuning the basal activity and the initial activation of T cells, opening up advanced possibilities for clinical interventions.

RESULTS

P2X4 and P2X7 are involved in the formation of initial Ca^{2+} microdomains in primary T cells

To analyze the impact of P2X4 and P2X7 on initial Ca^{2+} microdomains, we used a high-resolution Ca^{2+} live-cell imaging system with an acquisition rate of 40 frames/s (*8*, *9*) and freshly isolated primary $CD4^+$ T cells from wild-type (WT), *P2rx4*$^{-/-}$ and *P2rx7*$^{-/-}$ mice on a BALB/c background (*21*). Cells were stimulated with anti-CD3/anti-CD28–coated beads to mimic an immune synapse and stimulation via TCR/CD3 complex plus costimulation via CD28 (further termed TCR/CD3 stimulation). Initial Ca^{2+} microdomains were analyzed in a period from 0.5 s before and up to 15 s after bead contact (Fig. 1A). Directly (50 to 100 ms) after bead contact, WT T cells (Fig. 1A, top) showed increasing Ca^{2+} signals, starting with single local Ca^{2+} microdomains at the bead contact site and resulting in Ca^{2+} events spreading through the whole cell after 15 s. In contrast, T cells from *P2rx4*$^{-/-}$ and *P2rx7*$^{-/-}$ mice (Fig. 1A, middle and bottom) showed decreased Ca^{2+} microdomains directly in the initial period after bead contact. Ca^{2+} microdomains in the first 15 s occurred in 82% of the WT cells with an amplitude of 329 ± 14 nM and a frequency of approximately 0.29 signals per frame, which is equivalent to 12 signals per second. In *P2rx4*$^{-/-}$ and *P2rx7*$^{-/-}$ T cells, microdomains only occurred in 55 and 66% of the cells, with a significantly lower frequency of approximately 0.08 signals per frame (3 signals per second) and 0.1 signals per frame (5 signals per second; Fig. 1B). Moreover, the Ca^{2+} signals from *P2rx4*$^{-/-}$ T cells had a significantly lower amplitude of 266 ± 7 nM compared to the WT cells. By analyzing every 5 to 25 s after TCR stimulation (Fig. 1C), we observed a significantly decreased number of Ca^{2+} signals for cells from *P2rx4*$^{-/-}$ between 5 and 25 s after TCR stimulation, whereas cells from *P2rx7*$^{-/-}$ mice only show significantly decreased Ca^{2+} signals between 5 and 10 s compared to WT cells. The number of these highly dynamic Ca^{2+} microdomains directly at the artificial immune synapse was also decreased in the KOs 50 to 100 ms after stimulation compared to the WT (Fig. 1D), revealing an impact of P2X4 and P2X7 on Ca^{2+} microdomains tens of milliseconds after T cell stimulation.

Next, we compared the differences obtained by gene KOs (WT versus *P2rx4*$^{-/-}$ or *P2rx7*$^{-/-}$) to pharmacological inhibition using the chemical inhibitors for P2X4, 5-BDBD (*22*, *23*) (fig. S1) and PSB-15417 (*24*) (Fig. 2), and the inhibitory nanobody against P2X7, 13A7-dim-Alb (*19*) (Fig. 2). In control cells, Ca^{2+} microdomains occurred again directly (50 to 100 ms) after bead contact, whereas cells with inhibited P2X4 or P2X7 channels just show a few Ca^{2+} signals (Fig. 2A). In the first 15 s upon TCR stimulation, the Ca^{2+} microdomains were significantly decreased for both P2X4- and P2X7-inhibited cells, compared to the respective controls (Fig. 2B). The amplitude of the Ca^{2+} microdomains from cells upon P2X4 inhibition was again significantly reduced (Fig. 2B). The significantly decreased number of Ca^{2+} microdomains by inhibition of P2X4 and P2X7 as well as the decreased amplitude in cells upon P2X4 inhibition are in line with the results from P2X4 and P2X7 KO mice (Fig. 1).

Furthermore, between 2.5 s before and up to 25 s after TCR stimulation, a significant and consistent decrease of Ca^{2+} signals for the cells with inhibition of P2X4 (Fig. 2C, left) and P2X7 (Fig. 2C, right) was observed.

To analyze Ca^{2+} entry at the artificial immune synapse, we further compared Ca^{2+} microdomains in the outer sublayer of the cells at the contact site with the stimulating beads. The number of signals upon P2X4 and P2X7 inhibition was significantly reduced after TCR/CD3 stimulation compared to controls (Fig. 2D). Our results of P2X4 inhibition by PSB-15417 were confirmed with a second inhibitor for this channel, 5-BDBD (fig. S1). Here, we also observed significantly reduced Ca^{2+} signals in the first 15 s after TCR/CD3 stimulation (fig. S1B) as well as directly after stimulation at the artificial immune synapse (fig. S1D). These results substantiate that initial Ca^{2+} entry events were driven by P2X4 and P2X7 channels, leading to the question of interaction of the two channels during this initial phase. P2X4 and P2X7 show the highest sequence similarity compared to other P2X family members, and the *P2rx4* gene is located downstream of the *P2rx7* gene on the same chromosome (*25*, *26*). Moreover, homotrimers of P2X7 were already coimmunoprecipitated with P2X4 in macrophages, and Boumechache and colleagues (*27*) suggested an interaction of the channels inside the receptor complexes. To analyze colocalization during the formation of initial Ca^{2+} signals at the plasma membrane, superresolution imaging with optical reassignment (SoRa) was performed using directly conjugated nanobodies with the fluorophores CF568 and A647 against P2X4 and P2X7. Colocalization of the proteins was analyzed only at the plasma membrane of T cells to study the impact of interaction of P2X4 and P2X7 on Ca^{2+} influx (fig. S2A). During the basal state without stimulation, P2X4 and P2X7 proteins located at the plasma membrane show a slight colocalization of about 11%, and after a short (10-s) activation with soluble anti-CD3, colocalization increased to 15% (fig. S2B). In the first 10 s after stimulation of the cells, no significant increase in colocalization was observed, but after a longer activation time of 5 min, a significantly increased colocalization of P2X4 and P2X7 was observed (fig. S2B). These results indicate the interaction of P2X4 and P2X7 during global Ca^{2+} events, but for the generation of the initial Ca^{2+} microdomains, an extensive interaction of P2X4 and P2X7 seems not to be necessary.

Next, we analyze downstream signaling in *P2rx4*$^{-/-}$ or *P2rx7*$^{-/-}$ $CD4^+$ T cells, as it was reported that $CD4^+$ T cells from mice showed decreased migration upon inhibition of P2X4 and, to a lesser extent, P2X7 and P2X1 channels (*20*). Accordingly, we observed a significantly decreased and delayed global Ca^{2+} response after T cell stimulation with soluble anti-CD3 in *P2rx4*$^{-/-}$ and *P2rx7*$^{-/-}$ compared to $CD4^+$ WT cells (fig. S3, A to C). This further correlates with decreased expression of immediate early gene Nur77 after 18 hours for which the expression level closely reflects the strength of TCR stimulation (*28*) and decreased proliferation of $CD4^+$ T cells for *P2rx7*$^{-/-}$; however, expression of activation marker CD69 was not affected (fig. S3, D to H).

Immediate ATP release following TCR stimulation activates P2X4 and P2X7

P2X4 and P2X7 are activated by extracellular ATP binding to the channels, resulting in Ca^{2+} influx into T cell (*16*, *17*, *29*). Do we observe the same effects as above in Figs. 1 and 2 by removing the P2X4 and P2X7 channel activator, the extracellular ATP? To address this

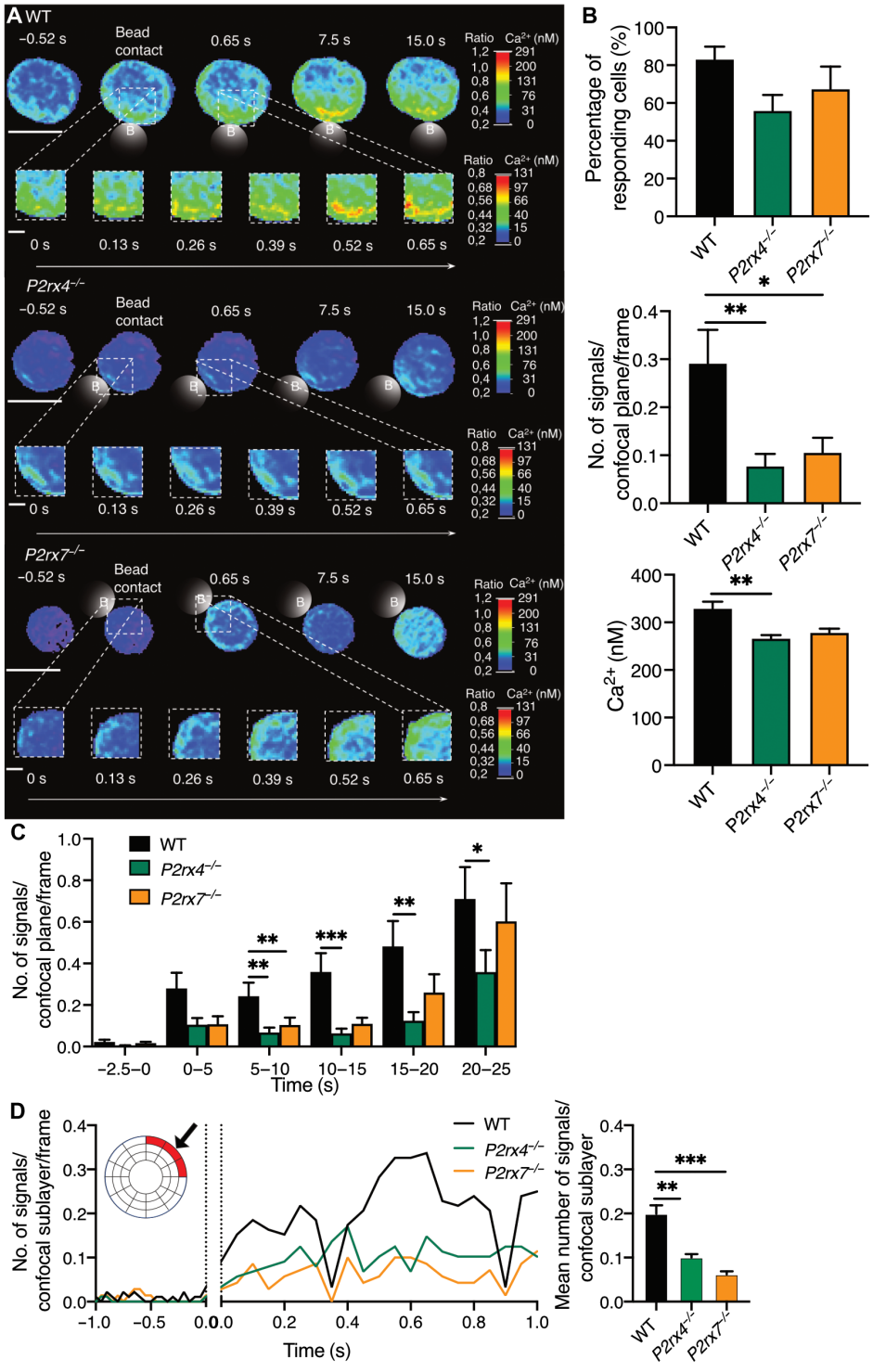

Fig. 1. Decreased Ca^{2+} microdomains in T cells from *P2rx4*$^{-/-}$ and *P2rx7*$^{-/-}$ KO mice. Ca^{2+} imaging of $CD4^+$ T cells of WT or *P2rx4*$^{-/-}$ and *P2rx7*$^{-/-}$ mice. Cells were stimulated with anti-CD3/anti-CD28–coated beads. A minimum of 10 different mice were used. (B to D) Data are means ± SEM; WT, $n = 46$ cells; *P2rx4*$^{-/-}$, $n = 47$ cells; *P2rx7*$^{-/-}$, $n = 39$ cells. Statistical analysis by Kruskal-Wallis test. (**A**) Representative cells of WT or *P2rx4*$^{-/-}$ and *P2rx7*$^{-/-}$ were shown for 0.52 s before and up to 15 s after stimulation with anti-CD3/anti-CD28–coated beads (scale bar, 5 μm) as well as for 0 to 0.65 s in 0.13-s steps zoomed into the region of bead contact (scale bar, 1 μm). (**B**) Quantification of the first 15 s after bead contact for $CD4^+$ T cells of WT or *P2rx4*$^{-/-}$ and *P2rx7*$^{-/-}$ mice. The percentage of responding cells, the number of Ca^{2+} microdomains per frame for whole cells (confocal plane), and the average Ca^{2+} concentration of these signals are shown. (**C**) Quantification of the number of Ca^{2+} microdomains per frame for the period 2.5 to 0 s before and every 5 s after bead contact up to 25 s after bead contact. (**D**) Analysis of the Ca^{2+} microdomains in the first second before and after TCR stimulation for the sublayers at the contact site (as indicated in red) (left). Quantification of the signals in the first second after bead contact (right). *$P < 0.05$, **$P < 0.005$, ***$P < 0.001$.

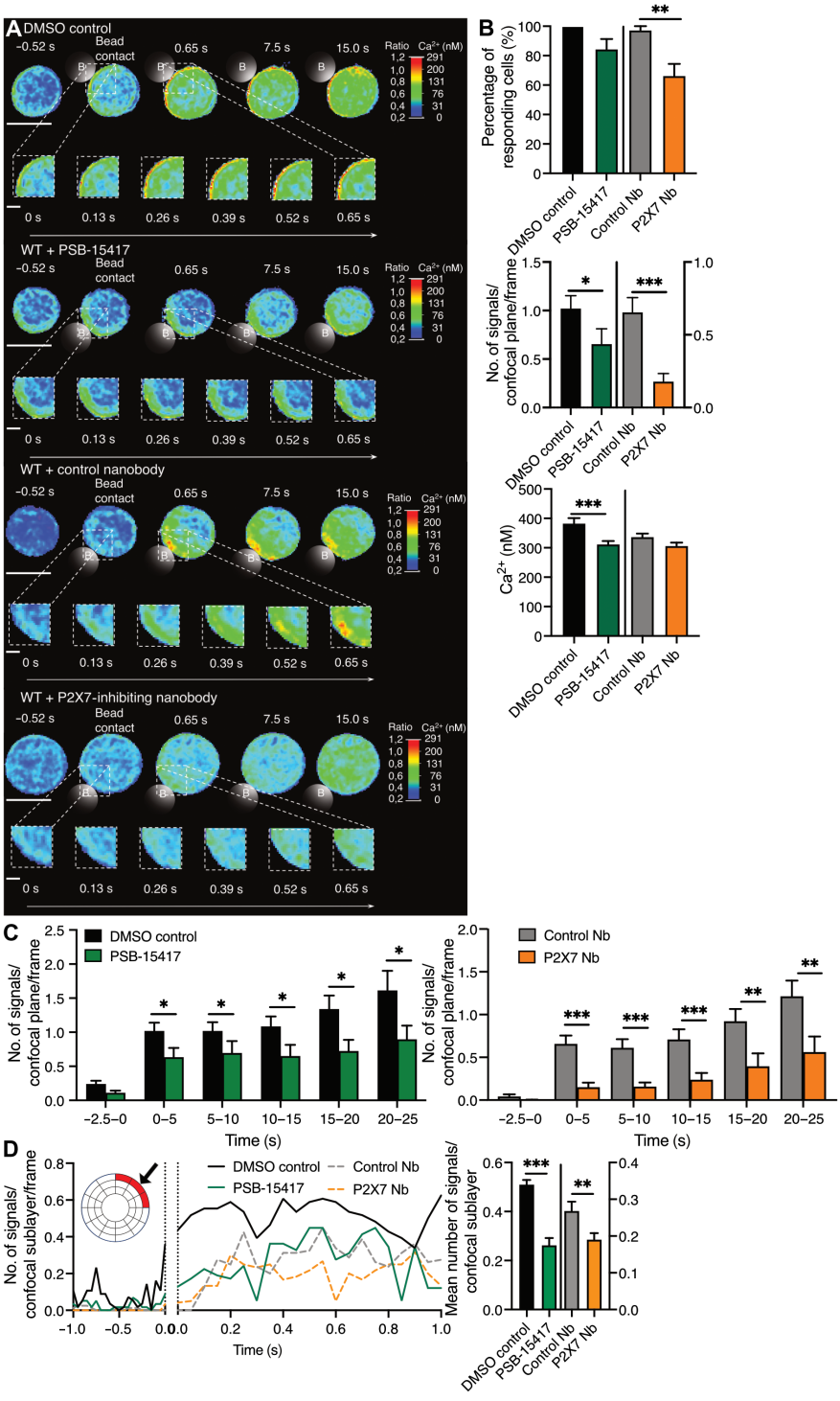

Fig. 2. Reduced Ca^{2+} microdomains in T cells with directly inhibited P2X4 and P2X7 channels. Ca^{2+} imaging of $CD4^+$ T cells of WT mice incubated with or without PSB-15417 (1 μM) for the inhibition of P2X4 or inhibiting nanobody (P2X7-Nb) 13A7-dim-Alb (1 μg/ml) for the inhibition of P2X7. A dimethyl sulfoxide (DMSO) control (0.01%) or an irrelevant nanobody (Control Nb; dummy-dim-Alb, 1 μg/ml) was used. Cells were stimulated with anti-CD3/anti-CD28–coated beads. A minimum of five different mice were used. (B to D) Data are means ± SEM; DMSO control, $n = 28$ cells; control nanobody, $n = 40$; cells treated with PSB-15417, $n = 29$ cells; cells treated with the P2X7-inhibiting nanobody, $n = 30$ cells. Statistical analysis by an unpaired two-tailed Mann-Whitney test. (**A**) , inhibited P2X4 and P2X7 channels were shown for 0.52 s before and up to 15 s after stimulation with anti-CD3/anti-CD28–coated beads (scale bar, 5 μm) as well as for 0 to 0.65 s in 0.13-s steps zoomed into the region of bead contact (scale bar, 1 μm). (**B**) Quantification of the first 15 s after bead contact for $CD4^+$ T cells of controls or inhibited P2X4 and P2X7. (**C**) Quantification of the number of Ca^{2+} microdomains per frame for the period 2.5 to 0 s before and every 5 s after bead contact up to 25 s after bead contact. DMSO control and cells treated with PSB-15417 were compared (left), as well as the control Nb with the P2X7-Nb (right). (**D**) Analysis of the Ca^{2+} microdomains in the first second before and after TCR stimulation for the sublayers at the contact site (as indicated in red) (left). Quantification of the signals in the first second after bead contact (right). *$P < 0.05$, **$P < 0.005$, ***$P < 0.001$.

question, we added apyrase, which hydrolyzes tri- and diphosphate groups of nucleotides (*30*, *31*). Three minutes before Ca^{2+} imaging, WT $CD4^+$ T cells were incubated with apyrase (10 U/ml). After 1 min of measurement, we stimulated the cells with anti-CD3/anti-CD28–coated beads. WT cells without apyrase incubation showed local Ca^{2+} microdomains increasing more and more after 15 s after bead contact through the cell (Fig. 3A, top). In comparison, cells treated with apyrase showed decreased local Ca^{2+} microdomains (Fig. 3A, bottom). In the first 15 s after activation in cells treated with apyrase, microdomains occurred with a significantly decreased frequency compared to the WT (WT, approximately 0.97 signals per frame; apyrase, approximately 0.25 signals per frame; Fig. 3B). In addition, investigating 5-s periods after TCR/CD3 stimulation also significantly reduced Ca^{2+} signals in cells treated with apyrase between 0 and 25 s compared to WT T cells not treated with apyrase that were observed (Fig. 3C). We conclude that the missing extracellular ATP because of degradation by apyrase (Fig. 3) resulted in decreased numbers of initial Ca^{2+} microdomains. As control, the same experiment was carried out using apyrase that was inactivated by boiling for 30 min (fig. S3). T cells incubated with boiled apyrase did not show any altered Ca^{2+} response (fig. S4). These results suggest a very fast release of ATP into the extracellular space. In addition, directly at the artificial immune synapse, we observed a reduced number of Ca^{2+} microdomains tens of milliseconds after stimulation in cells incubated with apyrase (Fig. 3D). Thus, ATP seems to be released immediately after stimulation of T cells, promoting the activation of the purinergic channels P2X4 and P2X7 to generate Ca^{2+} microdomains during the initial phase of Ca^{2+} signaling.

To further understand the mechanism of ATP release, we started to treat WT $CD4^+$ T cells with a mimetic inhibitor peptide for PANX1, termed ^{10}panx1. PANX1 is part of a family of glycoproteins, consisting of three family members PANX1 to PANX3 (*32*), expressed in $CD4^+$ T cells (*33*) acting as the main ATP-releasing channel (*34*, *35*). A typical T cell treated with the PANX1 inhibitor showed less Ca^{2+} signals after bead contact than the WT cell in the first 0.65 s and at the later time point of 15 s after T cell stimulation (Fig. 4A, top). Zoomed into the artificial immune synapse seconds after stimulation, only very few signals were detected for cells treated with ^{10}panx1 (Fig. 4A, bottom). Quantifying the first 15 s after bead contact, Ca^{2+} microdomains were significantly reduced in cells treated with ^{10}panx1 compared to WT T cells (Fig. 4B). To compare the temporal role of ATP release and the activation of the P2X channels in relation to the formation of Ca^{2+} microdomains, the number of Ca^{2+} microdomains was again analyzed 2.5 s before and in 5-s steps after T cell stimulation (Fig. 4C). T cells with reduced ATP release due to the inhibition of PANX1 showed significantly decreased Ca^{2+} signals between 0 and 5 s, 5 and 10 s, and 10 and 15 s. The initial Ca^{2+} microdomains at the artificial immune synapse significantly decreased in T cells treated with ^{10}panx1 compared to WT T cells already in the first second after bead contact (Fig. 4D). Together, T cells reveal a very fast apyrase- or ^{10}panx1-sensitive ATP release into the extracellular space via PANX1, which is responsible for the activation of P2X4 and P2X7, resulting in the amplification of initial Ca^{2+} microdomains.

Basal ATP release via PANX1 activates P2X4 in unstimulated T cells

To understand the fine-tuning of the Ca^{2+} signals after T cell stimulation, Diercks *et al.* (*9*) showed in 2018 that lower and less frequent Ca^{2+} microdomains in the absence of TCR/CD3 stimulation were already produced by preformed clusters of STIM1 and ORAI1. Therefore, we analyzed these Ca^{2+} microdomains using a high-resolution Ca^{2+} live-cell imaging system (*8*, *9*) in P2X4 and P2X7 KO T cells, in cells treated with the P2X4 inhibitor PSB-15417, or in cells treated with the PANX1 inhibitor ^{10}panx1 in the absence of TCR/CD3 stimulation (Fig. 5, A to C). Ca^{2+} microdomains occurred in nonstimulated WT or control T cells already with a lower frequency of approximately 0.07 to 0.2 signals per frame compared to Ca^{2+} microdomains upon TCR/CD3 stimulation with a frequency of approximately 0.3 to 1.0 signals per frame (Figs. 1 to 4B and 5, A to C, number of signals per confocal plane per frame). P2X4 KO cells showed, in the absence of TCR/CD3 stimulation, significantly reduced Ca^{2+} microdomain numbers during a 15-s period without stimulation, whereas *P2rx7*$^{-/-}$ cells showed no altered Ca^{2+} response compared to WT cells (Fig. 5A). The amplitude of the signals in *P2rx7*$^{-/-}$ T cells did not show differences to WT cells. Ca^{2+} signals were also significantly reduced in cells upon P2X4 inhibition by PSB-15417 (*24*), but the amplitude of the signals was not altered (Fig. 5B).

These results indicate a role of P2X4, but not of P2X7, in basal Ca^{2+} signaling in T cells in the absence of TCR/CD3 stimulation. Moreover, we demonstrate that the autocrine release of ATP is responsible for activating P2X4 in unstimulated cells by inhibiting the ATP release channel PANX1. In T cells treated with ^{10}panx1, the number and amplitude of Ca^{2+} signals were significantly decreased compared to the WT (Fig. 5C).

Together, the results reveal two different mechanisms, one for T cells in the absence of TCR/CD3 stimulation and one for the first seconds in activated T cells (Fig. 6, A and B). In the absence of TCR/CD3 stimulation, lower and less frequent Ca^{2+} microdomains (Figs. 5, A to C, and 6A) were promoted via STIM1 and ORAI1 (*9*), resulting in the activation of PANX1 (*36*, *37*). Subsequently, a low basal ATP release via PANX1 activates P2X4. After TCR/CD3 activation, increasing ATP release triggers not only P2X4 but now also the less sensitive P2X7 channel (*38*), leading to the formation of Ca^{2+} microdomains within tens of milliseconds (Figs. 1, 2, and 6B) comparable to our previous model of Ca^{2+} microdomain formation due to RYR1 or ORAI1 and STIM1/2 (*8*–*10*).

DISCUSSION

T cell Ca^{2+} microdomains are evoked upon TCR/CD3 stimulation by the production of NAADP that binds to HN1L/JPT2 and targets RYR1, as well as clusters of STIM1/2 with ORAI1 (*8*–*10*). Using specific inhibitors and cells from suitable KO mice, we identified two purinergic cation channels, namely, P2X4 and P2X7, which are involved in forming initial Ca^{2+} microdomains in tens of milliseconds after TCR/CD3 stimulation. In a similar setup to our experiments, a reduced number of Ca^{2+} microdomains within the first second after TCR/CD3 stimulation was demonstrated for *Orai1*$^{-/-}$, *Stim1*$^{-/-}$, *Stim2*$^{-/-}$, and *Stim1*$^{-/-}$/*2*$^{-/-}$ as well as *Ryr1*$^{-/-}$ T cells or by NAADP antagonism by BZ194 (*9*) and recently by knocking out the NAADP receptor HN1L/JPT2 (*10*). The interaction between STIM1/2 and ORAI1/2/3 and the alteration in Ca^{2+} signaling profiles (*9*) are predicted to have an important influence on downstream effects, like the activation of the nuclear factor of activated T cells (NFAT) (*39*). It was shown that the loss of either STIM1 or STIM2 impairs both the formation of Ca^{2+} microdomains (*9*) and translocation of NFAT1

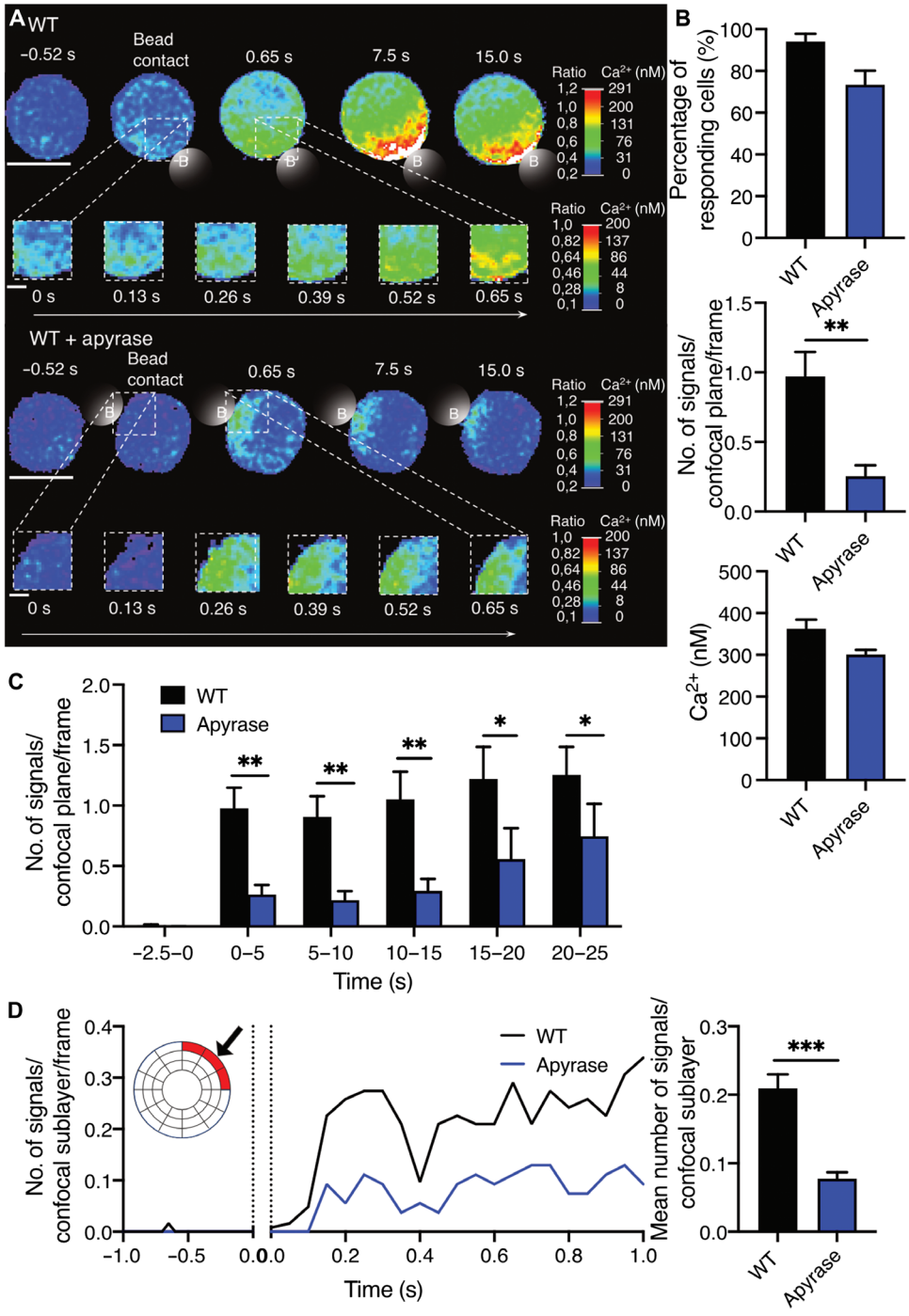

Fig. 3. Removal of extracellular ATP decreases Ca^{2+} microdomains. Ca^{2+} imaging of $CD4^+$ T cells of WT mice incubated with or without 10 U of apyrase. Cells were stimulated with anti-CD3/anti-CD28–coated beads. A minimum of five different mice were used. (B to D) Data are means ± SEM; WT, $n = 31$ cells; cells treated with apyrase, $n = 27$ cells. Statistical analysis was done using a nonparametric unpaired two-tailed Mann-Whitney test. (**A**) Representative cells of WT or cells treated with apyrase were shown for 0.52 s before and up to 15 s after stimulation with anti-CD3/anti-CD28–coated beads (scale bar, 5 μm) as well as for 0 to 0.65 s in 0.13-s steps zoomed into the region of bead contact (scale bar, 1 μm). (**B**) Quantification of the first 15 s after bead contact for $CD4^+$ T cells of WT or cells treated with apyrase. The percentage of responding cells, the number of Ca^{2+} microdomains per frame for whole cells (confocal plane), and the average Ca^{2+} concentration of these signals are shown. (**C**) Quantification of the number of Ca^{2+} microdomains per frame for the period 2.5 to 0 s before and every 5 s after bead contact up to 25 s after bead contact. (**D**) Analysis of the Ca^{2+} microdomains in the first second before and after TCR stimulation for the sublayers at the contact site (as indicated in red) (left). Quantification of the signals in the first second after bead contact (right). $^*P < 0.05$, $^{**}P < 0.005$, $^{***}P < 0.001$.

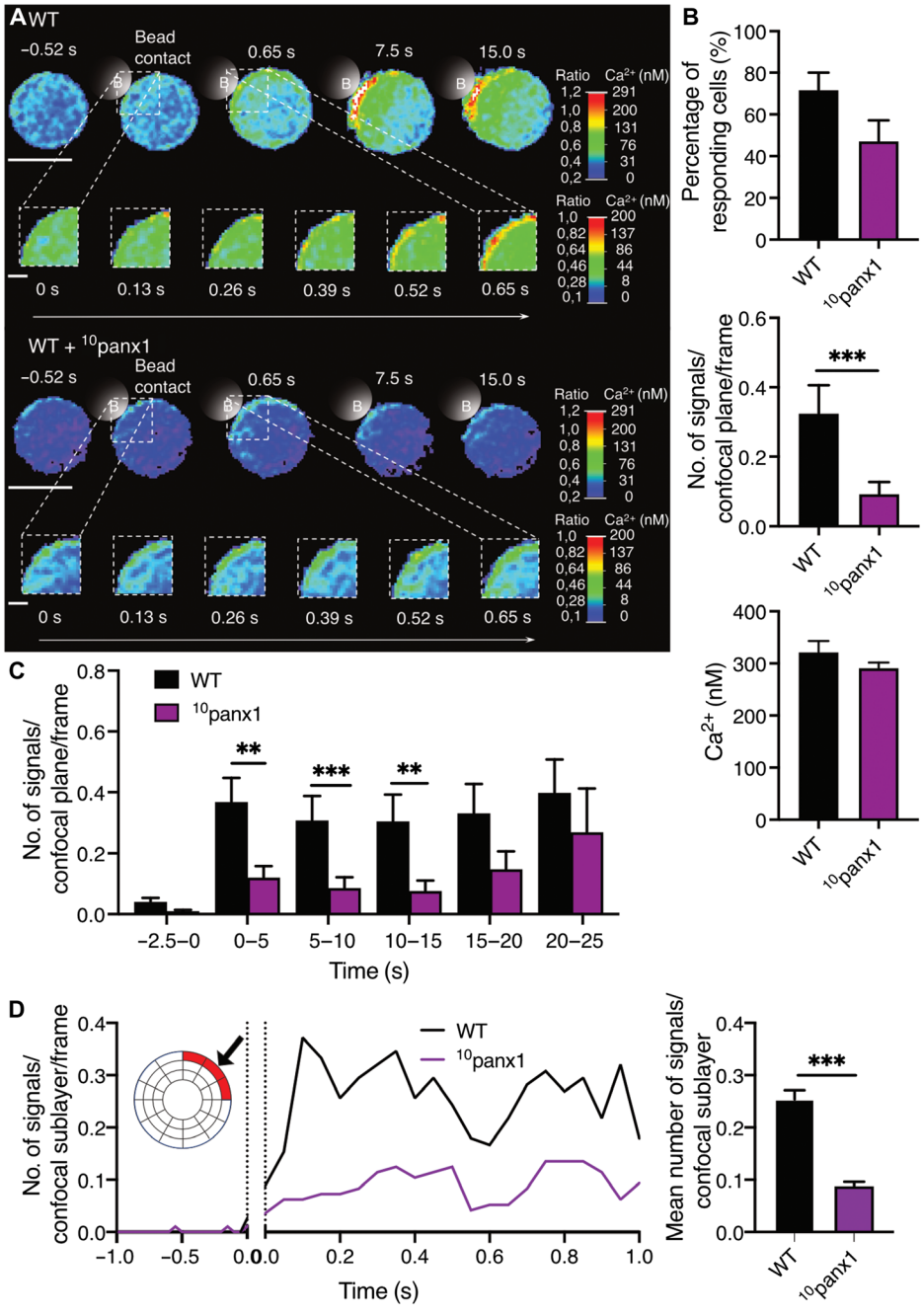

Fig. 4. Inhibition of PANX1 reduces the formation of Ca^{2+} microdomains. Ca^{2+} imaging of $CD4^+$ T cells of WT mice incubated with or without 200 μM PANX1 inhibitor ^{10}panx1 20 min before measurements. Cells were stimulated with anti-CD3/anti-CD28–coated beads. A minimum of 10 different mice were used. (B to D) Data are means ± SEM; WT, $n = 39$ cells; cells treated with ^{10}panx1, $n = 48$ cells. Statistical analysis by an unpaired two-tailed Mann-Whitney test. (**A**) Representative cells of WT or cells treated with ^{10}panx1 were shown for 0.52 s before and up to 15 s after stimulation with anti-CD3/anti-CD28–coated beads for whole cells (scale bar, 5 μm) as well as for 0 to 0.65 s in 0.13-s steps zoomed into the region of bead contact (scale bar, 1 μm). (**B**) Quantification of the first 15 s after bead contact for $CD4^+$ T cells of WT or cells treated with ^{10}panx1. The percentage of responding cells, the number of Ca^{2+} microdomains per frame for whole cells (confocal plane), and the average Ca^{2+} concentration of these signals are shown. (**C**) Quantification of the number of Ca^{2+} microdomains per frame for the period 2.5 to 0 s before and every 5 s after bead contact up to 25 s after bead contact. (**D**) Analysis of the Ca^{2+} microdomains in the first second before and after TCR stimulation for the sublayers at the contact site (as indicated in red) (left). Quantification of the signals in the first second after bead contact (right). $^{**}P < 0.005$, $^{***}P < 0.001$.

and NFAT4 (*40*). Furthermore, antagonizing NAADP by BZ194 results in decreased translocation of NFAT and attenuated clinical scores in rat experimental autoimmune encephalomyelitis (*6*, *41*). NFAT activation is also known to be triggered by purinergic signaling, and loss of P2X7 resulted in diminished NFAT activation (*17*, *42*, *43*). The similarities of downstream effects and alteration in initial Ca^{2+} signaling between the known channels involved in early T cell activation and the two purinergic cation channels P2X4 and P2X7

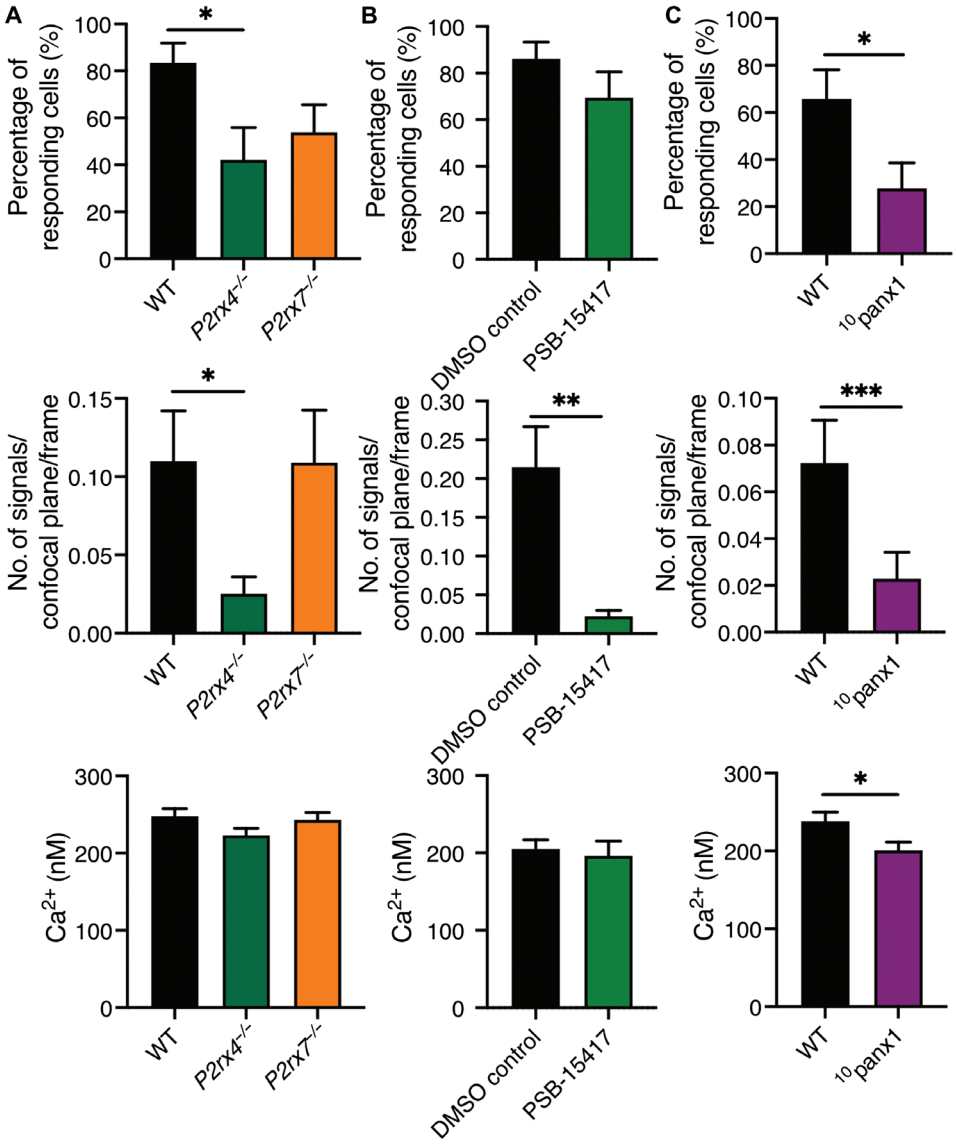

Fig. 5. Basal ATP release via PANX1 activates P2X4, promoting the formation of Ca^{2+} microdomains in the absence of TCR/CD3 stimulation. Ca^{2+} imaging of $CD4^+$ T cells of WT mice or *P2rx4*$^{-/-}$ and *P2rx7*$^{-/-}$ mice. WT cells were incubated with or without PSB-15417 (1 μM) for the inhibition of P2X4 or 200 μM PANX1 inhibitor ^{10}panx1 20 min before measurements. For the P2X4-inhibiting compound, a DMSO control (0.01%) was used. A minimum of four different mice were used. (A to C) Percentage of responding cells, number of Ca^{2+} microdomains per frame for whole cells (confocal plane), and average Ca^{2+} concentration of these signals. Data are means ± SEM; statistical analysis was done by a Kruskal-Wallis test or an unpaired two-tailed Mann-Whitney test. (**A**) Quantification of 15 s without stimulation for $CD4^+$ T cells of WT or *P2rx4*$^{-/-}$ and *P2rx7*$^{-/-}$ mice. WT, $n = 44$ cells; *P2rx4*$^{-/-}$, $n = 45$ cells; *P2rx7*$^{-/-}$, $n = 52$ cells. (**B**) Quantification of 15 s without stimulation for $CD4^+$ T cells of a DMSO control or cells treated with PSB-15417. DMSO control, $n = 35$ cells; cells treated with PSB-15417, $n = 26$ cells. (**C**) Quantification of 15 s without stimulation for $CD4^+$ T cells of WT or cells treated with ^{10}panx1. WT, $n = 40$ cells; cells treated with ^{10}panx1, $n = 47$ cells. *$P < 0.05$, **$P < 0.005$, ***$P < 0.001$.

analyzed in this study are notable. Thus, we need to expand our model of initial T cell activation, including the purinergic pathway on a level equivalent to SOCE and NAADP signaling (Fig. 6B). Upon TCR stimulation, not only the NAADP/HN1L-JPT2/RYR1 axis together with SOCE through STIM1/2 and ORAI1 but also P2X4 and P2X7 are involved in the formation of initial Ca^{2+} microdomains.

An interplay of SOCE with purinergic signaling was already found by Woehrle and colleagues (*16*) in Jurkat T cells, revealing colocalization of ORAI1 and STIM1 with P2X4 within 30 min of stimulation at the immune synapse. The low colocalization of P2X4 and P2X7 during the formation of initial Ca^{2+} microdomains before and after T cell stimulation in the current study indicates no interaction of these channels in the basal state of T cells and the first tens of milliseconds after TCR stimulation. In contrast, at later time points, an increased colocalization was observed, consistent with earlier studies (*27*, *44*). It was not confirmed that P2X4 and P2X7 form stable heteromers (*45*), and a mutual interaction for global Ca^{2+} signals could be assumed because of the impact of both channels on later stages of Ca^{2+} signaling (*12*–*14*, *16*–*18*, *46*) and the increased colocalization of P2X4 and P2X7 after 5 min of TCR stimulation (fig. S2). In addition, we showed the influence of both channels on the initial steps of T cell activation and Ca^{2+} microdomain formation,

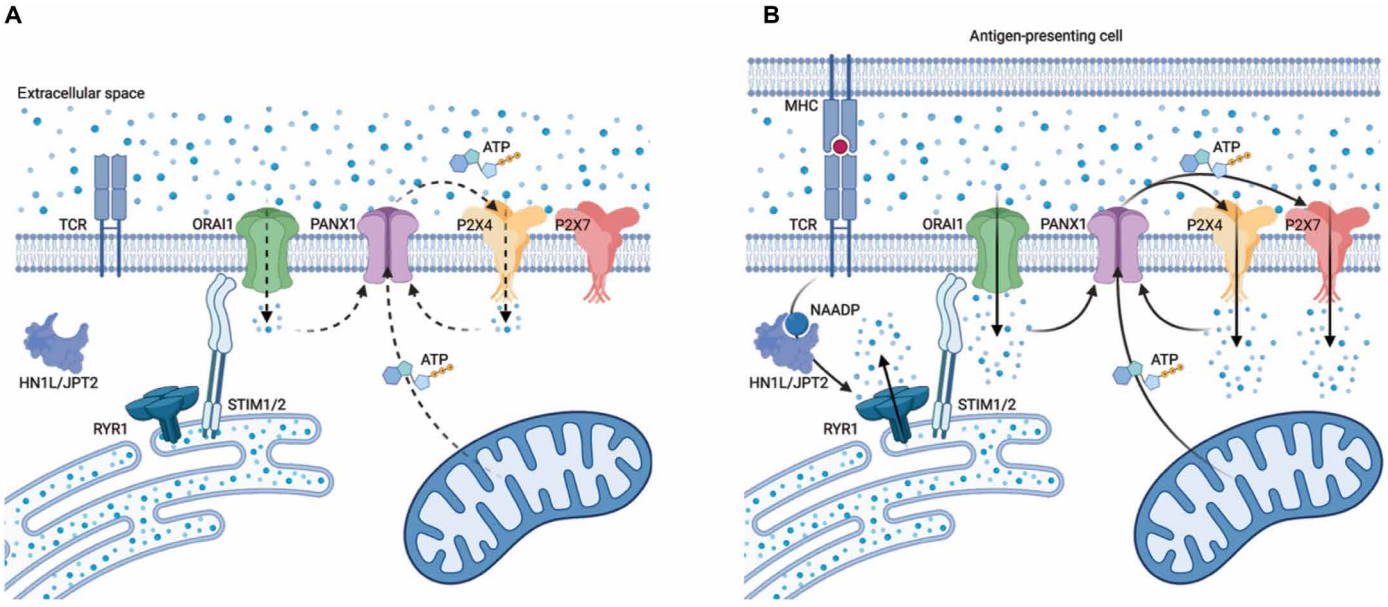

Fig. 6. Summary of Ca^{2+} microdomain formation in preactivated state and milliseconds after T cell activation. Ca^{2+} signaling before and milliseconds after stimulation of the TCR. Blue dots indicate Ca^{2+} signals, and dotted arrows indicate lower amounts of Ca^{2+} or ATP compared to solid arrows. Figures were created with BioRender. (**A**) A basal activity of T cells is due to preformed clusters of STIM1 and ORAI1 resulting in lower and less frequent Ca^{2+} microdomains. PANX1 is probably activated by these Ca^{2+} microdomains and releases low concentrations of ATP, which activates the sensitive purinergic channel P2X4, which also results in lower and less frequent Ca^{2+} microdomains. (**B**) Upon TCR stimulation, on the one hand, RYR1 is activated, probably by NAADP bound to HN1L/JPT2, resulting in local and transient Ca^{2+}release. NAADP-evoked Ca^{2+} release through RYR1 contributes directly to highly dynamic Ca^{2+} microdomains and promotes the activation of STIM1/2 and thus SOCE through ORAI1 channels, leading to an amplification of initial Ca^{2+} microdomains. On the other hand, increasing Ca^{2+} concentrations foster ATP release via PANX1 upon TCR stimulation, which activates P2X4 and the less sensitive P2X7 channel in an autocrine manner, and further promote again an amplification of initial Ca^{2+} microdomains.

but only P2X4 seems to be necessary for basal T cell activity without TCR/CD3 stimulation. Together, the results of colocalization and Ca^{2+} imaging indicate different time slots of P2X4 and P2X7 activity. Whereas P2X4 seems to be already active during antigen-presenting cell (APC) recognition and initial T cell activation, P2X7 is activated not until the initial TCR/CD3 stimulation. The different activation periods of P2X4 and P2X7 may influence downstream mechanisms, such as cytokine expression, T cell migration, or proliferation.

Several downstream effects in mice were previously described, for example, by Ulmann and co-workers (*47*) for P2X4 and Chessell and co-workers (*48*) for P2X7, who analyzed prostaglandin E_2 and different cytokine levels, like interleukin-6 (IL-6), in *P2rx4*$^{-/-}$ or *P2rx7*$^{-/-}$ mice after induced inflammatory pain, suggesting a prominent role of both purinergic channels during initial inflammatory signaling pathways. In human Jurkat T cells with silenced *P2rx4* or *P2rx7*, IL-2 transcription after stimulation with anti-CD3/anti-CD28–coated beads showed a significantly lower response (*16*, *17*). Moreover, inhibition of P2X4 and, to a lesser extent, P2X7 or P2X1 leads to decreased proliferation, and only inhibition of P2X4 reduced the migration of $CD4^+$ T cells from mice (*20*). When combining these published and our own data, the following model was generated: Initial Ca^{2+} microdomains of *P2rx4*$^{-/-}$ or *P2rx7*$^{-/-}$ T cells are decreased in the first tens of milliseconds after T cell stimulation, resulting in a delayed global Ca^{2+} response within minutes and decreased expression of the activation marker Nur77 after 18 hours, apparently translating into reduced proliferation in *P2rx7*$^{-/-}$ (fig. S3, G and H) and migration of T cells upon P2X4 inhibition (*20*).

ATP acts as an essential extracellular signaling molecule, with a crucial role in many cellular processes like cell-to-cell communication, inducing apoptosis, inflammatory reactions, or tumor growth (*49*–*53*). For example, human $CD4^+$ T cells incubated with 250 nM ATP showed increased secretion of cytokines like IL-2 (*52*). Our study suggests that ATP release through PANX1 activates P2X4 and P2X7 channels in an autocrine fashion (Figs. 3 and 4), consistent with earlier investigations (*16*, *46*, *54*, *55*). Hence, removal of extracellular ATP or inhibition of ATP release significantly decreased initial Ca^{2+} microdomains that were observed in tens of milliseconds after TCR/CD3 stimulation (Figs. 3D and 4D), revealing a very fast release of ATP and activation of the two P2X channels. Mitochondrial ATP production and release were also shown for this early time period after T cell stimulation (*18*), once more connecting Ca^{2+} signaling to purinergic signaling, whereby ATP production in the mitochondria depends on initial Ca^{2+} signaling in T cells (*56*, *57*).

More insights into the kinetics of this complex process were obtained by analyzing Ca^{2+} microdomains in T cells in the absence of TCR/CD3 stimulation. The fast release of ATP can be explained by the basal activity of PANX1 activating P2X4 to promote Ca^{2+} microdomains (Fig. 5C). After TCR/CD3 stimulation, the ATP release seems to be fostered to fully activate P2X4 and the less sensitive P2X7 channel (*38*) to promote Ca^{2+} microdomains. A basal T cell activity was also shown by preclustered STIM1 and ORAI1, promoting Ca^{2+} microdomains with lower amplitude and frequency already before T cell stimulation (*9*). We are now able to show the involvement of basal ATP release because of PANX1, resulting in P2X4 activation and the formation of less frequent Ca^{2+} microdomains in unstimulated T cells (Fig. 5, A to C). A basal mitochondrial ATP production in unstimulated cells claimed by Ledderose and colleagues (*58*) supports our findings of basal ATP release via PANX1

and preactivation of P2X4. Moreover, another purinergic channel, P2X1, was recently implicated in this basal phase of $CD4^+$ T cell function, being activated by lower ATP concentrations than P2X4 or P2X7 (*58*). In unstimulated Jurkat T cells, P2X1 and P2X7 act on the activity of mitochondria to produce ATP, revealing a positive feedback loop of purinergic signaling during basal T cell activity (*59*). The importance of the precisely regulated ATP homeostasis is elucidated in cancer cells. Here, the fine-tuning of extracellular ATP concentrations through the purinergic axis of P2X4, P2X7, and PANX1 can decide between a pathway of survival and tumor growth and a P2X7-mediated cell death (*59*–*61*). Different ATP concentrations induce different cellular responses. While ATP in the lower nanomolar range (1 to 50 nM) does not alter either proliferation or cell death of activated conventional $CD4^+$ T cells and regulatory T cells, intermediate concentrations of ATP (250 nM) result in the activation of conventional $CD4^+$ T cells. High concentrations (1 mM) of ATP decrease expression of CD54, CD49d, and CD25 during activation of conventional $CD4^+$ T cells but enhance proliferation, adhesion capacity, and migration of regulatory T cells (*52*). A low permanent ATP release in unstimulated T cells and the formation of Ca^{2+} microdomains might be necessary, or at least supportive, for a fast immune response and APC recognition. To this end, the interaction of purinergic and Ca^{2+} signaling in T cells not stimulated via the TCR/CD3 complex might be an early step of the immune response to be targeted for development of therapeutic interventions. One issue needs to be addressed at this point: There is a huge difference in the sensitivity to ATP concentrations in humans and mice. Cell death is induced in mice by ATP concentrations in the micromolar range, whereas in humans millimolar concentrations are needed (*62*). One possible explanation might be the missing P2Y11 channel in mice (*63*). P2Y11 inhibits the P2X7-dependent pore formation and, to this end, P2X7-mediated cell death, but not Ca^{2+} signaling (*64*). Interaction between P2X and P2Y receptors seems to be adjustable key in ATP balance; P2X1 activity, for example, was shown to be potentiated by coexpression with P2Y1 and P2Y2 (*65*). P2X and P2Y interactions during Ca^{2+} signaling and microdomain formation require further investigations, and the difference between human and mouse channel expression needs to be kept in mind.

In conclusion, we identify a previously unknown function of P2X4 that is required for the formation of Ca^{2+} microdomains in the absence of TCR/CD3 stimulation, probably via a low basal ATP release via PANX1 (Fig. 6A). Moreover, we show that both P2X4 and P2X7 have a central role in initial Ca^{2+} microdomain formation (Fig. 6B) already in tens of milliseconds after T cell stimulation, because these Ca^{2+} microdomains were blocked by hydrolyzing extracellular ATP or blocking PANX1. There are several mechanisms of PANX1 activation (*35*), but how PANX1 is activated during basal T cell activity is still unclear and needs to be addressed in further investigations. It was recently described that PANX1 is activated by increasing Ca^{2+} concentrations (*36*, *37*). To this end, the activation of PANX1 in the absence of TCR/CD3 stimulation might be due to preclustered STIM1 and ORAI1 promoting Ca^{2+} microdomains (*9*).

MATERIALS AND METHODS

Study design

The aim of the study was to analyze the influence of purinergic signaling on the formation of Ca^{2+} microdomains in T cells. Primary murine $CD4^+$ T cells were used, and Ca^{2+} imaging was done in cells with pharmacological or genetic inhibition of P2X4, P2X7, or PANX1 channels. Ca^{2+} microdomain acquisition and detection was performed as previously described (*66*). The Ca^{2+} microdomain detection threshold for microdomains after activation was set to 112 nM and for microdomains without TCR/CD3 stimulation to 90 nM Ca^{2+}. T cells with global and not spatiotemporally restricted Ca^{2+} amplitudes above the threshold of 90 nM were considered as preactivated and not included in this study. Colocalization of P2X4 and P2X7 before and after T cell activation was analyzed using SoRa. Downstream effects were analyzed in WT and genetically inhibited P2X4 and P2X7 $CD4^+$ T cells using flow cytometry. All Ca^{2+} imaging experiments were done three or more times to achieve cell numbers of a minimum of 20. All other experiments were done three times.

Reagents

The Ca^{2+} indicators Fluo4-AM and FuraRed-AM were obtained from Life Technologies. They were dissolved in dimethyl sulfoxide (DMSO), and aliquots were stored at −20°C until measurements. The monoclonal antibodies (mAbs) anti-mouse CD3 and anti-mouse CD28 were obtained from BD Biosciences. The inhibiting compound 5-BDBD was purchased from Tocris; PSB-15417 was provided by C. Müller (Department of Pharmacy, University of Bonn); and the P2X7-inhibiting nanobody 13A7-dim-Alb and the control nanobody dummy-dim-Alb (*19*) as well as directly conjugated nanobodies against P2X4 (dimer + CF568) and P2X7 (dimer + A647) were provided by F. Koch-Nolte (Department of Immunology, University Medical Centre Hamburg Eppendorf). All other reagents were ordered from Sigma-Aldrich.

Animal models

$P2rx4^{-/-}$ ($P2rx4^{tm1Rass}$; MGI (Mouse Genome Informatics):3665297) and $P2rx7^{-/-}$ mice ($P2rx7^{tm1Gab}$; MGI:2386080) were backcrossed for 13 generations onto the BALB/c background and were used for experiments along with WT BALB/c mice. All mice were bred at the animal facility of the University Medical Center (UKE). All experiments involving tissue derived from animals were performed with the approval of the responsible regulatory committee (Hamburger Behörde für Gesundheit und Verbraucherschutz, Veterinärwesen/Lebensmittelsicherheit, ORG 941).

Isolation of primary T cells

T cells were isolated from freshly dissected spleens and lymph nodes of WT or KO mice on a BALB/c background. The spleens and lymph nodes were ground through a cell strainer (Ø 40 μm) using the upturned plunger of a syringe in 30 ml of RPMI 1640 containing 25 mM Hepes and GlutaMAX-1 (Gibco, Life Technologies), adding penicillin and streptomycin (100 U/ml) and 7.5% (v/v) newborn calf serum (Biochrom, Merck Millipore). Cell suspension was centrifuged (1200 rpm, 5 min, 4°C), and the cell pellet was dissolved in 5 ml of ammonium-chloride-potassium buffer [4.3 g of ammonium chloride, 0.5 g of $KHCO_3$, and 0.0186 g of Na_2-EDTA in 400 ml of H_2O (pH 7.2 to 7.4)] for 3 to 5 min for lysis of the erythrocytes. After incubation, the lysis was stopped by adding 25 ml of RPMI medium and by centrifuging at 1200 rpm, 5 min, and 4°C. The supernatant was discarded, and cell pellet was dissolved in 2 ml of Dulbecco's phosphate-buffered saline (DPBS) without $CaCl_2$ and $MgCl_2$ (Gibco, Life Technologies). $CD4^+$ T cells were isolated using a negative selection kit according to the manufacturer's protocol (EasySep Mouse $CD4^+$ T Cell Enrichment Kit, STEMCELL

Technologies Inc.). The purity of cells was analyzed by fluorescence-activated cell sorting (FACS) and was up to 97 to 98%.

Local Ca^{2+} imaging in primary T cells and Ca^{2+} microdomain detection

Freshly isolated $CD4^+$ T cells from WT or *P2rx4*$^{-/-}$ or *P2rx7*$^{-/-}$ mice were loaded in RPMI (see above) with the two Ca^{2+} dyes Fluo4 (10 μM) and FuraRed (20 μM), and Ca^{2+} imaging with a frame rate of 40 frames/s was done as described in detail by Diercks *et al.* (*66*). Cells were resuspended in Ca^{2+} buffer [140 mM NaCl, 5 mM KCl, 1 mM $MgSO_4$, 1 mM $CaCl_2$, 20 mM Hepes (pH 7.4), 1 mM NaH_2PO_4, and 5 mM glucose] and imaged for 3 min on coverslips coated with 5 μl of bovine serum albumin (BSA) (5 mg/ml) and 5 μl of poly-L-lysine (0.1 mg/ml). After the first minute, they were either stimulated or not stimulated with anti-CD3/anti-CD28–coated beads adding 10 μl of the bead solution with a pipette, and Ca^{2+} changes were recorded for the last 2 min of measurements. During the postprocessing, all T cells were normalized on bead contact site and time.

For direct inhibition of P2X4 and P2X7, cells were incubated for 30 min before the Ca^{2+} measurements with a P2X4-inhibiting compound (5-BDBD, 10 μM) as well as PSB-15417 (1 μM) or a P2X7-inhibiting nanobody (13A7-dim-Alb, 1 μg/ml). The compounds were resolved in DMSO; to this end, a DMSO control (0.01 and 0.1%) for the measurements was used, as well as a nanobody control (dummy-dim-Alb; 1 μg/ml) for the measurements with the inhibiting nanobody. The addition of apyrase (10 U/ml) 3 min before measurements was used to remove the extracellular ATP. Moreover, a negative control was produced by heating the apyrase up for 30 min at 70°C. To inhibit the PANX1 hemichannel, cells were incubated with the PANX1 mimetic peptide ^{10}panx1 (*67*) at a concentration of 200 μM for 20 min.

Ca^{2+} microdomains, defined as small, compact connected sets of pixels with high $[Ca^{2+}]_i$ values, were detected with a threshold of 112 nM in cells activated with anti-CD3/anti-CD28–coated beads or without stimulation with a threshold of 90 nM in an automated MATLAB script (*66*). To analyze Ca^{2+} microdomains developing close to the bead contact (as shown in Figs. 1D to 4D), the cell shapes were approximated to be circular, all cells of the considered group/condition rotated such that the bead contact sites agreed for the cells, and the cell areas were subdivided in a dartboard-like manner detailed in (*66*). Ca^{2+} microdomain statistics (number of microdomains, associated Ca^{2+} concentration) were then computed for the different dartboard compartments and specified time windows. For Figs. 1D to 4D, the three outer compartments at the bead contact site that are highlighted in red in figures were analyzed.

Colocalization analysis with SoRa

Primary $CD4^+$ T cells from BALB/c mice were left unstimulated or stimulated with soluble anti-CD3 (0.5 mg/ml) for 10 s or 5 min and were seeded on slides coated with poly-L-lysine (0.1 mg/ml). The cells were fixed with 4% (w/v) paraformaldehyde (Alfa Aesar) for 15 min and permeabilized with 0.05% (v/v) saponin (Fluka) again for 15 min. They were incubated overnight at 4°C with 10% (v/v) of fetal bovine serum to block unspecific binding sites. Cells were stained with directly conjugated nanobodies against P2X4 (dimer + CF568; 1:50) and P2X7 (dimer +A647; 1:50) (provided by T. Stähler, Department of Immunology, University Medical Centre Hamburg Eppendorf) for 1 hour. Slides with fixed cells were mounted on coverslips upside down with Abberior Mount solid at 4°C overnight. Image acquisition was done using a superresolution spinning disk microscope (Visitron), a CSU-W1 SoRa optic (2.8×; Yokogawa), a ×100 magnification objective (Zeiss), and a scientific Complementary metal–oxide–semiconductor camera (Orca-Flash 4.0, C13440-20CU, Hamamatsu). The following lasers and filters were used: aP2X4-CF568: excitation, 561 nm laser; emission filter, 609/54 nm; aP2X7-A647: excitation, 640 nm laser; emission, 700/75 nm. Image deconvolution was based on the principle of Arigovindan *et al.* (*68*) [reimplemented and adapted by Woelk *et al.* (*69*)]. For colocalization analysis, the trainable weka (Waikato environment for knowledge analysis) segmentation plugin and a watershed segmentation were used in FIJI (version 2.1.0/1.53c) to improve the separation of the single proteins, which were detected. Only proteins near the plasma membrane were analyzed for colocalization. For the calculation and quantification of the colocalization of P2X4 and P2X7, a MATLAB script, based on the published study by Nauth *et al.* (*70*), was used.

Global Ca^{2+} imaging in primary T cells

Freshly isolated $CD4^+$ T cells from WT, *P2rx4*$^{-/-}$, or *P2rx7*$^{-/-}$ mice were loaded in 500 μl of RPMI (see above) with 4 μM Fura2-AM for 35 min at 37°C. After 20 min of incubation, 2 ml of medium was added. After Fura2 loading, cells were washed with Ca^{2+} buffer [140 mM NaCl, 5 mM KCl, 1 mM $MgSO_4$, 1 mM $CaCl_2$, 1 mM NaH_2PO_4, 20 mM Hepes, and 5.5 mM glucose (pH 7.4) (NaOH), sterile-filtered] (*10*). Ca^{2+} imaging was performed using a Leica IRBE microscope equipped with a 40-fold objective and an electron-multiplying charge-coupled device camera (C9100-13, Hamamatsu). As a light source, a Sutter DG-4 High Speed Wavelength Switcher with the following filter set was used: excitation, hard-coated (HC) 340/26 nm and HC 387/11 nm; beam splitter, 400DCLP; emission, 510/84 nm (*10*). Cells were imaged with an exposure time of 20 ms for 340 and 380 nm for 10 min on slides coated with 5 μl of BSA (5 mg/ml) and 5 μl of poly-L-lysine (0.1 mg/ml) and stimulated with 10 μl of soluble anti-CD3 after 2 min. Image acquisition was done in 16-bit mode with Volocity software (PerkinElmer), and postprocessing like background correction, splitting of the fluorescence channels, and selection of the regions of interest was performed with FIJI software (version 2.1.0/1.53c).

Flow cytometry

Spleen cells were isolated by pressing the organ successively through 70- and 40-μm cell strainers. Erythrocytes were depleted with lysis buffer [155 mM NH_4Cl, 10 mM $KHCO_3$, 10 μM EDTA (pH 7.2)]. Cells were incubated in 500 μl of Iscove's modified Dulbecco's medium (IMDM) supplemented with fetal calf serum, glutamine, gentamicin, and 2-mercaptoethanol. Cells were simulated for 18 hours with anti-CD3ε mAb (1 μg/ml; clone 145-2C11, BioLegend, San Diego, CA) and anti-CD28 mAb (1 μg/ml; clone 37.51, BioLegend). For extracellular antibody staining, cells were incubated in PBS with 1% rat serum and anti–Fc receptor mAb (10 μg/ml) (clone 2.4G2, BioXCell, West Lebanon, NH). Cells were incubated with a fixable dead cell stain (Alexa Flour 750 carboxylic acid, succinimidyl ester, Invitrogen, Eugene, OR), AF700-conjugated anti-CD4 mAb (clone RM4-5, BioLegend), and BV605-conjugated anti-CD69 mAb (clone H1.2F3, BioLegend) for 20 min on ice. Intracellular antibody staining was conducted with the Foxp3/Transcription Factor Staining Buffer Set (Invitrogen) according to the manufacturer's protocol. Cells were stained with phycoerythrin-conjugated anti-NUR77 mAb (clone 12.14, Invitrogen). Cells were analyzed using a FACSCelesta flow

cytometer (BD Biosciences, Franklin Lakes, NJ) and FlowJo software (Tree Star, Ashland, OR).

For the proliferation assay, spleen cells were incubated for 10 min at room temperature with carboxyfluorescein diacetate succinimidyl ester (CFSE) proliferation dye (5 μM; Invitrogen). The cells were washed twice and then incubated with anti-CD3ε mAb (1 μg/ml; clone 145-2C11, BioLegend) and anti-CD28 mAb (1 μg/ml; clone 37.51, BioLegend) in supplemented IMDM. After 3 days, cells were stained with APC-conjugated anti-CD4 mAb (clone RM4-5, eBioscience, San Diego, CA) and a fixable dead cell stain (Alexa Flour 750 carboxylic acid, succinimidyl ester, Invitrogen) and analyzed by FACS.

Statistics

All data are presented as means ± SEM of independent experiments performed as at least triplicates. Data were analyzed using MATLAB software (MathWorks) and Prism 9 (GraphPad Software). Groups were compared using Mann-Whitney *U* or Kruskal-Wallis tests or two-way analysis of variance (ANOVA) and Dunnett's multiple comparisons test. A *P* value of 0.05 was considered as significant.

SUPPLEMENTARY MATERIALS

Supplementary material for this article is available at https://science.org/doi/10.1126/sciadv.abl9770

View/request a protocol for this paper from *Bio-protocol*.

REFERENCES AND NOTES

1. R. Fliegert, J. Heeren, F. Koch-Nolte, V. O. Nikolaev, C. Lohr, C. Meier, A. H. Guse, Adenine nucleotides as paracrine mediators and intracellular second messengers in immunity and inflammation. *Biochem. Soc. Trans.* **47**, 329–337 (2019).
2. M. Trebak, J. P. Kinet, Calcium signalling in T cells. *Nat. Rev. Immunol.* **19**, 154–169 (2019).
3. S. D. Guile, L. Alcaraz, T. N. Birkinshaw, K. C. Bowers, M. R. Ebden, M. Furber, M. J. Stocks, Antagonists of the P2X(7) receptor. From lead identification to drug development. *J. Med. Chem.* **52**, 3123–3141 (2009).
4. E. C. Keystone, M. M. Wang, M. Layton, S. Hollis, I. B. McInnes, Clinical evaluation of the efficacy of the *P2X7* purinergic receptor antagonist AZD9056 on the signs and symptoms of rheumatoid arthritis in patients with active disease despite treatment with methotrexate or sulphasalazine. *Ann. Rheum. Dis.* **71**, 1630–1635 (2012).
5. M. Vaeth, J. Yang, M. Yamashita, I. Zee, M. Eckstein, C. Knosp, U. Kaufmann, P. K. Jani, R. S. Lacruz, V. Flockerzi, I. Kacskovics, M. Prakriya, S. Feske, ORAI2 modulates store-operated calcium entry and T cell-mediated immunity. *Nat. Commun.* **8**, 14714 (2017).
6. C. Cordiglieri, F. Odoardi, B. Zhang, M. Nebel, N. Kawakami, W. E. F. Klinkert, D. Lodygin, F. Lühder, E. Breunig, D. Schild, V. K. Ulaganathan, K. Dornmair, W. Dammermann, B. V. L. Potter, A. H. Guse, A. Flügel, Nicotinic acid adenine dinucleotide phosphate-mediated calcium signalling in effector T cells regulates autoimmunity of the central nervous system. *Brain* **133**, 1930–1943 (2010).
7. A. Guse, I. Ernst, R. Fliegert, NAADP signaling revisited. *Curr. Top. Med. Chem.* **13**, 2978–2990 (2013).
8. I. M. A. Wolf, B. P. Diercks, E. Gattkowski, F. Czarniak, J. Kempski, R. Werner, D. Schetelig, H. W. Mittrücker, V. Schumacher, M. Von Osten, D. Lodygin, A. Flügel, R. Fliegert, A. H. Guse, Frontrunners of T cell activation: Initial, localized Ca2+ signals mediated by NAADP and the type 1 ryanodine receptor. *Sci. Signal.* **8**, ra102 (2015).
9. B. P. Diercks, R. Werner, P. Weidemüller, F. Czarniak, L. Hernandez, C. Lehmann, A. Rosche, A. Krüger, U. Kaufmann, M. Vaeth, A. V. Failla, B. Zobiak, F. I. Kandil, D. Schetelig, A. Ruthenbeck, C. Meier, D. Lodygin, A. Flügel, D. Ren, I. M. A. Wolf, S. Feske, A. H. Guse, ORAI1, STIM1/2, and RYR1 shape subsecond Ca^{2+} microdomains upon T cell activation. *Sci. Signal.* **11**, eaat0358 (2018).
10. H. G. Roggenkamp, I. Khansahib, C. L. C. Hernandez, Y. Zhang, D. Lodygin, A. Krüger, F. Gu, F. Möckl, A. Löhndorf, V. Wolters, D. Woike, A. Rosche, A. Bauche, D. Schetelig, R. Werner, H. Schlüter, A. V. Failla, C. Meier, R. Fliegert, T. F. Walseth, A. Flügel, B. P. Diercks, A. H. Guse, HN1L/JPT2: A signaling protein that connects NAADP generation to Ca^{2+} microdomain formation. *Sci. Signal.* **14**, eabd5647 (2021).
11. G. S. Gunaratne, E. Brailoiu, S. He, E. M. Unterwald, S. Patel, J. T. Slama, T. F. Walseth, J. S. Marchant, Essential requirement for JPT2 in NAADP-evoked Ca^{2+} signaling. *Sci. Signal.* **14**, eabd5605 (2021).
12. U. Schenk, A. M. Westendorf, E. Radaelli, A. Casati, M. Ferro, M. Fumagalli, C. Verderio, J. Buer, E. Scanziani, F. Grassi, Purinergic control of T cell activation by ATP released through pannexin-1 hemichannels. *Sci. Signal.* **1**, ra6 (2008).
13. G. Burnstock, J. M. Boeynaems, Purinergic signalling and immune cells. *Purinergic Signal.* **10**, 529–564 (2014).
14. V. M. Ruiz-Rodríguez, J. D. Cortes-García, M. de Jesús Briones-Espinoza, E. Rodríguez-Varela, M. Vega-Cárdenas, A. Gómez-Otero, M. H. García-Hernández, D. P. Portales-Pérez, P2X4 receptor as a modulator in the function of P2X receptor in CD4+ T cells from peripheral blood and adipose tissue. *Mol. Immunol.* **112**, 369–377 (2019).
15. F. Grassi, The P2X7 receptor as regulator of T cell development and function. *Front. Immunol.* **11**, 1179 (2020).
16. T. Woehrle, L. Yip, A. Elkhal, Y. Sumi, Y. Chen, Y. Yao, P. A. Insel, W. G. Junger, Pannexin-1 hemichannel-mediated ATP release together with P2X1 and P2X4 receptors regulate T-cell activation at the immune synapse. *Blood* **116**, 3475–3484 (2010).
17. L. Yip, T. Woehrle, R. Corriden, M. Hirsh, Y. Chen, Y. Inoue, V. Ferrari, P. A. Insel, W. G. Junger, Autocrine regulation of T-cell activation by ATP release and P2X 7 receptors. *FASEB J.* **23**, 1685–1693 (2009).
18. C. Ledderose, Y. Bao, M. Lidicky, J. Zipperle, L. Li, K. Strasser, N. I. Shapiro, W. G. Junger, Mitochondria are gate-keepers of T cell function by producing the ATP that drives purinergic signaling. *J. Biol. Chem.* **289**, 25936–25945 (2014).
19. W. Danquah, M. S. Catherine, B. Rissiek, C. Pinto, S. P. Arnau, M. Amadi, D. Iacenda, J. H. Knop, A. Hammel, P. Bergmann, N. Schwarz, J. Assunção, W. Rotthier, F. Haag, E. Tolosa, P. Bannas, B. G. Eric, T. Magnus, T. Laeremans, C. Stortelers, F. Koch-Nolte, Nanobodies that block gating of the P2X7 ion channel ameliorate inflammation. *Sci. Transl. Med.* **8**, 366ra162 (2016).
20. C. Ledderose, K. Liu, Y. Kondo, C. J. Slubowski, T. Dertnig, S. Denicoló, M. Arbab, J. Hubner, K. Konrad, M. Fakhari, J. A. Lederer, S. C. Robson, G. A. Visner, W. G. Junger, Purinergic P2X4 receptors and mitochondrial ATP production regulate T cell migration. *J. Clin. Invest.* **128**, 3583–3594 (2018).
21. M. Er-Lukowiak, Y. Duan, F. Rassendren, L. Ulmann, A. Nicke, F. Ufer, M. A. Friese, F. Koch-Nolte, T. Magnus, B. Rissiek, A *P2rx7* passenger mutation affects the vitality and function of T cells in congenic mice. *iScience* **23**, 101870 (2020).
22. B. Balázs, T. Dankó, G. Kovács, L. Köles, M. A. Hediger, Á. Zsembery, Investigation of the inhibitory effects of the benzodiazepine derivative, 5-BDBD on P2X 4 purinergic receptors by two complementary methods. *Cell. Physiol. Biochem.* **32**, 11–24 (2013).
23. C. Coddou, R. Sandoval, M. J. Hevia, S. S. Stojilkovic, Characterization of the antagonist actions of 5-BDBD at the rat P2X4 receptor. *Neurosci. Lett.* **690**, 219–224 (2019).
24. A. Abdelrahman, V. Namasivayam, S. Hinz, A. C. Schiedel, M. Köse, M. Burton, A. El-Tayeb, M. Gillard, J. Bajorath, M. de Ryck, C. E. Müller, Characterization of P2X4 receptor agonists and antagonists by calcium influx and radioligand binding studies. *Biochem. Pharmacol.* **125**, 41–54 (2017).
25. Z. Hou, J. Cao, Comparative study of the P2X gene family in animals and plants. *Purinergic Signal.* **12**, 269–281 (2016).
26. R. Kopp, A. Krautloher, A. Ramírez-Fernández, A. Nicke, P2X7 interactions and signaling—Making head or tail of it. *Front. Mol. Neurosci.* **12**, 183 (2019).
27. M. Boumechache, M. Masin, J. M. Edwardson, D. Górecki, R. Murrell-Lagnado, Analysis of assembly and trafficking of native P2X4 and P2X7 receptor complexes in rodent immune cells. *J. Biol. Chem.* **284**, 13446–13454 (2009).
28. J. F. Ashouri, A. Weiss, Endogenous Nur77 is a specific indicator of antigen receptor signaling in human T and B cells. *J. Immunol.* **198**, 657–668 (2017).
29. F. Di Virgilio, P. Chiozzi, D. Ferrari, S. Falzoni, J. M. Sanz, A. Morelli, M. Torboli, G. Bolognesi, O. R. Baricordi, Nucleotide receptors: An emerging family of regulatory molecules in blood cells. *Blood* **97**, 587–600 (2001).
30. M. Handa, G. Guidotti, Purification and cloning of a soluble ATP-diphosphohydrolase (Apyrase) from potato tubers (Solanum tuberosum). *Biochem. Biophys. Res. Commun.* **218**, 916–923 (1996).
31. M. Tsukimoto, A. Tokunaga, H. Harada, S. Kojima, Blockade of murine T cell activation by antagonists of P2Y6 and P2X7 receptors. *Biochem. Biophys. Res. Commun.* **384**, 512–518 (2009).
32. R. Bruzzone, S. G. Hormuzdi, M. T. Barbe, A. Herb, H. Monyer, Pannexins, a family of gap junction proteins expressed in brain. *Proc. Natl. Acad. Sci. U.S.A.* **100**, 13644–13649 (2003).
33. K. F. Shoji, P. J. Sáez, P. A. Harcha, H. L. Aguila, J. C. Sáez, Pannexin1 channels act downstream of P2X7 receptors in ATP-induced murine T-cell death. *Channels* **8**, 142–156 (2014).
34. W. G. Junger, Immune cell regulation by autocrine purinergic signalling. *Nat. Rev. Immunol.* **11**, 201–212 (2011).
35. Y. H. Chiu, M. S. Schappe, B. N. Desai, D. A. Bayliss, Revisiting multimodal activation and channel properties of Pannexin 1. *J. Gen. Physiol.* **150**, 19–39 (2018).
36. P. Whyte-Fagundes, G. Zoidl, Mechanisms of pannexin1 channel gating and regulation. *Biochim. Biophys. Acta Biomembr.* **1860**, 65–71 (2018).
37. K. A. Taylor, J. R. Wright, M. P. Mahaut-Smith, Regulation of Pannexin-1 channel activity. *Biochem. Soc. Trans.* **43**, 502–507 (2015).

38. K. Kaczmarek-Hájek, É. Lörinczi, R. Hausmann, A. Nicke, Molecular and functional properties of P2X receptors-recent progress and persisting challenges. *Purinergic Signal.* **8**, 375–417 (2012).
39. Y. Gwack, S. Feske, S. Srikanth, P. G. Hogan, A. Rao, Signalling to transcription: Store-operated Ca^{2+} entry and NFAT activation in lymphocytes. *Cell Calcium* **42**, 145–156 (2007).
40. S. M. Emrich, R. E. Yoast, P. Xin, J. Sneyd, D. I. Yule, S. M. Emrich, R. E. Yoast, P. Xin, V. Arige, L. E. Wagner, N. Hempel, D. L. Gill, Article. Omnitemporal choreographies of all five STIM / Orai and IP_3Rs underlie the complexity of mammalian ll Omnitemporal choreographies of all five STIM/Orai and IP_3Rs underlie the complexity of mammalian Ca^{2+} signaling. *CellReports* **34**, 108760 (2021).
41. W. Dammermann, B. Zhang, M. Nebel, C. Cordiglieri, F. Odoardi, T. Kirchberger, N. Kawakami, J. Dowden, F. Schmid, K. Dornmair, M. Hohenegger, A. Flügel, A. H. Guse, B. V. L. Potter, NAADP-mediated Ca^{2+} signaling via type 1 ryanodine receptor in T cells revealed by a synthetic NAADP antagonist. *Proc. Natl. Acad. Sci. U.S.A.* **106**, 10678–10683 (2009).
42. E. Adinolfi, A. L. Giuliani, E. De Marchi, A. Pegoraro, E. Orioli, F. Di Virgilio, The P2X7 receptor: A main player in inflammation. *Biochem. Pharmacol.* **151**, 234–244 (2018).
43. P. Prasai, G. C. Stefos, W. Becker, Extracellular ATP activates NFAT-dependent gene expression in neuronal PC12 cells via P2X receptors. *BMC Neurosci.* **12**, 90 (2011).
44. C. Guo, M. Masin, O. S. Qureshi, R. D. Murrell-Lagnado, Evidence for functional P2X4/P2X7 heteromeric receptors. *Mol. Pharmacol.* **72**, 1447–1456 (2007).
45. A. Nicke, Homotrimeric complexes are the dominant assembly state of native P2X7 subunits. *Biochem. Biophys. Res. Commun.* **377**, 803–808 (2008).
46. C. M. Wang, C. Ploia, F. Anselmi, A. Sarukhan, A. Viola, Adenosine triphosphate acts as a paracrine signaling molecule to reduce the motility of T cells. *EMBO J.* **33**, 1354–1364 (2014).
47. L. Ulmann, H. Hirbec, F. Rassendren, P2X4 receptors mediate PGE2 release by tissue-resident macrophages and initiate inflammatory pain. *EMBO J.* **29**, 2290–2300 (2010).
48. I. P. Chessell, J. P. Hatcher, C. Bountra, A. D. Michel, J. P. Hughes, P. Green, J. Egerton, M. Murfin, J. Richardson, W. L. Peck, C. B. A. Grahames, M. Anna, Y. Yiangou, R. Birch, P. Anand, G. N. Buell, Disruption of the *P2X7* purinoceptor gene abolishes chronic inflammatory and neuropathic pain. *Pain* **114**, 386–396 (2005).
49. M. V. Zamaraeva, R. Z. Sabirov, E. Maeno, Y. Ando-Akatsuka, S. V. Bessonova, Y. Okada, Cells die with increased cytosolic ATP during apoptosis: A bioluminescence study with intracellular luciferase. *Cell Death Differ.* **12**, 1390–1397 (2005).
50. P. Pellegatti, L. Raffaghello, G. Bianchi, F. Piccardi, V. Pistoia, F. Di Virgilio, Increased level of extracellular ATP at tumor sites: In vivo imaging with plasma membrane luciferase. *PLOS ONE* **3**, e2599 (2008).
51. J. Linden, F. Koch-Nolte, G. Dahl, Purine release, metabolism, and signaling in the inflammatory response. *Annu. Rev. Immunol.* **37**, 325–347 (2019).
52. S. Trabanelli, D. Očadlíková, S. Gulinelli, A. Curti, V. Salvestrini, R. de Paula Vieira, M. Idzko, F. Di Virgilio, D. Ferrari, R. M. Lemoli, Extracellular ATP exerts opposite effects on activated and regulatory $CD4^+$ T cells via purinergic P2 receptor activation. *J. Immunol.* **189**, 1303–1310 (2012).
53. T. M. Chused, S. Apasov, M. Sitkovsky, Murine T lymphocytes modulate activity of an ATP-activated P2Z-type purinoceptor during differentiation. *J. Immunol.* **157**, 1371–1380 (1996).
54. C. Ledderose, Y. Bao, J. Zhang, W. G. Junger, Novel method for real-time monitoring of ATP release reveals multiple phases of autocrine purinergic signalling during immune cell activation. *Acta Physiol.* **213**, 334–345 (2015).
55. Z. Deng, Z. He, G. Maksaev, R. M. Bitter, M. Rau, J. A. J. Fitzpatrick, P. Yuan, Cryo-EM structures of the ATP release channel pannexin 1. *Nat. Struct. Mol. Biol.* **27**, 373–381 (2020).
56. P. S. Brookes, Y. Yoon, J. L. Robotham, M. W. Anders, S. S. Sheu, Calcium, ATP, and ROS: A mitochondrial love-hate triangle. *Am. J. Physiol. Cell Physiol.* **287**, C817–C833 (2004).
57. C. J. Fox, P. S. Hammerman, C. B. Thompson, Fuel feeds function: Energy metabolism and the T-cell response. *Nat. Rev. Immunol.* **5**, 844–852 (2005).
58. C. Ledderose, Y. Bao, S. Ledderose, T. Woehrle, M. Heinisch, L. Yip, J. Zhang, S. C. Robson, N. I. Shapiro, W. G. Junger, Mitochondrial dysfunction, depleted purinergic signaling, and defective T cell vigilance and immune defense. *J. Infect. Dis.* **213**, 456–464 (2016).
59. C. Ledderose, T. Woehrle, S. Ledderose, K. Strasser, R. Seist, Y. Bao, J. Zhang, W. G. Junger, Cutting off the power: Inhibition of leukemia cell growth by pausing basal ATP release and P2X receptor signaling? *Purinergic Signal.* **12**, 439–451 (2016).
60. D. Draganov, S. Gopalakrishna-Pillai, Y. R. Chen, N. Zuckerman, S. Moeller, C. Wang, D. Ann, P. P. Lee, Modulation of P2X4/P2X7/Pannexin-1 sensitivity to extracellular ATP via Ivermectin induces a non-apoptotic and inflammatory form of cancer cell death. *Sci. Rep.* **5**, 16222 (2015).
61. O. Kepp, L. Bezu, T. Yamazaki, F. Di Virgilio, M. J. Smyth, G. Kroemer, L. Galluzzi, ATP and cancer immunosurveillance. *EMBO J.* e108130 (2021).
62. B. Rissiek, F. Haag, O. Boyer, F. Koch-Nolte, S. Adriouch, P2X7 on mouse T cells: One channel, many functions. *Front. Immunol.* **6**, 204 (2015).
63. K. Dreisig, B. R. Kornum, A critical look at the function of the P2Y11 receptor. *Purinergic Signal.* **12**, 427–437 (2016).
64. K. Dreisig, L. Sund, M. W. Dommer, N. P. Kristensen, K. Boddum, R. Viste, S. Fredholm, N. Odum, M. Jäättelä, S. Skov, B. R. Kornum, Human $P2Y_{11}$ expression level affects human P2X7 receptor-mediated cell death. *Front. Immunol.* **9**, 1159 (2018).
65. C. Vial, A. B. Tobin, R. J. Evans, G-protein-coupled receptor regulation of P2X1 receptors does not involve direct channel phosphorylation. *Biochem. J.* **382**, 101–110 (2004).
66. B. P. Diercks, R. Werner, D. Schetelig, I. M. A. Wolf, A. H. Guse, High-resolution calcium imaging method for local calcium signaling. *Methods Mol. Biol.* **1929**, 27–39 (2019).
67. P. Pelegrin, A. Surprenant, Pannexin-1 mediates large pore formation and interleukin-1β release by the ATP-gated P2X7 receptor. *EMBO J.* **25**, 5071–5082 (2006).
68. M. Arigovindan, J. C. Fung, D. Elnatan, V. Mennella, Y. H. M. Chan, M. Pollard, E. Branlund, J. W. Sedat, D. A. Agard, High-resolution restoration of 3D structures from widefield images with extreme low signal-to-noise-ratio. *Proc. Natl. Acad. Sci. U.S.A.* **110**, 17344–17349 (2013).
69. L. M. Woelk, S. A. Kannabiran, V. J. Brock, C. E. Gee, C. Lohr, A. H. Guse, B. P. Diercks, R. Werner, Time-dependent image restoration of low-SNR live-cell Ca2+ fluorescence microscopy data. *Int. J. Mol. Sci.* **22**, 11792 (2021).
70. T. Nauth, F. Huschka, M. Schweizer, J. B. Bosse, A. Diepold, A. V. Failla, A. Steffen, T. Stradal, M. Wolters, M. Aepfelbacher, Visualization of translocons in Yersinia type III protein secretion machines during host cell infection. *PLOS Pathog.* **14**, e1007527 (2018).

Acknowledgments: We acknowledge discussions with members of The Calcium Signalling Group and members of SFB 1328. Nb13A7 can be provided by F.K.-N. pending scientific review and a completed material transfer agreement. Requests for Nb13A7 should be submitted to nolte@uke.de. **Funding:** This work was supported by Deutsche Forschungsgemeinschaft (DFG) (project number 335447717; SFB 1328, project A01 to A.H.G.; project A02 to B.-P.D. and R.W.; project A03 to H.-W.M.; project A10 and Z01 to F.K.-N.; and project A11 to C.E.M.); Joachim-Herz-Stiftung (Hamburg), Infectophysics Consortium (project 4, to A.H.G.); NCL-Stiftung Hamburg (to A.H.G.); the Hamburg Ministry of Science, Research and Equality (LFF-FV75/0070-134, to A.H.G.); and University Medical Center Hamburg-Eppendorf (M3I consortium, to A.H.G.). **Author contributions:** Conceptualization: I.M.A.W., A.H.G., and B.-P.D. Methodology: V.J.B., B.-P.D., L.-M.W., R.W., M.E.-L., B.R., T.S., F.K.-N., and C.E.M. Investigation: V.J.B., M.E.-L., N.L., and T.S. Visualization: V.J.B., I.M.A.W., N.L., A.H.G., and B.-P.D. Funding acquisition: I.M.A.W., B.-P.D., R.W., A.H.G., F.K.-N., C.E.M., and H.-W.M. Supervision: B.-P.D., I.M.A.W., R.W., A.H.G., F.K.-N., C.E.M., and H.-W.M. Writing—original draft: V.J.B. Writing—review and editing: V.J.B., B.-P.D., A.H.G., R.W., B.R., and H.-W.M. **Competing interests:** F.K.-N. is the inventor on a patent related to this work, filed by the University Medical Center Hamburg-Eppendorf and Ablynx NV (WO2013178783, filed on 31 May 2013, published on 5 December 2013). The authors declare no other competing interests. **Data and materials availability:** All data needed to evaluate the conclusions in the paper are present in the paper and/or the Supplementary Materials.

Submitted 17 August 2021
Accepted 14 December 2021
Published 4 February 2022
10.1126/sciadv.abl9770